Power-law spectral decay as a general feature of spiral turbulence

Y. Soupart [1], M. G. Clerc,[2] and M. Tlidi [1]
[1]Département de Physique, Faculté des Sciences, Université libre de Bruxelles (U.L.B), C.P.231, 1050 Brussels, Belgium
[2]Departamento de física and Millennium Institute for Research in Optics, Facultad de Ciencias Físicas y Matemáticas, Universidad de Chile, Casilla 487-3, Santiago, Chile

(Received 26 August 2024; revised 26 January 2025; accepted 28 March 2025; published 12 May 2025)

Spiral waves emitted by topological defects and their instabilities are a fundamental and ubiquitous process in nature. We study this phenomenon using data from recent experiments and different prototype models ranging from coupled oscillators, reaction-diffusion, and nonlinear optics. Statistically we show that, for all systems considered, the spectral density exhibits a power-law decay on spatial scales shorter than the intrinsic wavelength. This reflects a common type of self-organization through a stationary turbulentlike dynamics. The role of short-range interactions due to high defects density is discussed. Using a generalized Hilbert transform in two dimensions, we show that local phase and amplitude field present similar power-law decays in their spectral density.

DOI: 10.1103/PhysRevResearch.7.023136

I. INTRODUCTION

Spiral waves are among the most common types of self-organized spatiotemporal behavior [1–3]. They are known to play an important role in many different biological processes, such as cardiac [4,5] and cerebral [6,7] activity, and cellular communication [8–12]. A spiral wave is a moving wavefront emitted from a curved free end that rotates around a center that constitutes a topological defect. Complex dynamics in spiral-forming systems is usually associated with defect-mediated turbulence, initially studied in the complex Ginzburg-Landau equation [13]. Based on the one-dimensional approximation of this model, Kuramoto and co-workers established the existence of a power-law spectrum in reduced variables, with a power-law extending over about a decade. He coined this behavior chemical turbulence [14,15]. This contrasts with the usual turbulence in fluid dynamics [16] where power-law spectra are observed over several decades due to the presence of structures (eddies) at different scales and the existence of a conservation law. Turbulentlike behaviors, such as chemical turbulence, were observed in different physical systems such as fiber lasers [17,18], nonlinear optics [19–21], active matter [22], interfacial dynamics [23], Bose-Einstein condensates [24], and financial markets [25]. In all these systems, a power-law decay behavior in the spectral density or probability distribution has been established for observables such as kinetic energy, light intensity, phase gradient, or price changes. Note that these power-laws typically range over (not more than) a decade due to the absence of different structures or defects at various scales and/or of a conserved quantity.

Here, we provide evidence for a general way in which systems exhibiting turbulencelike dynamics of spirals self-organize. A power-law decay at short-length scales in the average spectrum of the observable characterizes this spatial organization. Statistical analysis is first performed on experimental data consisting of a temporal sequence of the two-dimensional distribution of a chemical species concentration. Using a generalized two-dimensional Hilbert transform, the concentration field is then decomposed into a local phase and amplitude field, and their respective spectra are computed. These spectra similarly exhibit power laws at short spatial scales. Then, the generality of this feature is shown by performing the same analysis on various models exhibiting turbulentlike regimes of spirals stemming from different physical origins: coupled oscillators, reaction diffusion, and optical parametric oscillators.

II. EXPERIMENTAL OBSERVATION

Turbulentlike dynamics of chemical spiral waves of a signaling protein on the membrane of starfish egg cells were recently experimentally reported, see inset of Fig. 1(a). Details about this experiment can be found in [12,26]. Let us start by defining the average spectrum in the radial direction $\mathcal{F}[X](k)$. It is the temporal average of the two-dimensional Fourier spectrum over which angular averaging was performed. This yields a spectral density along the radial direction in the space of wavenumbers. Mathematically, denoting $k = |\boldsymbol{k}|$ the wavenumber,

$$\mathcal{F}[X](k) = \left\langle \int_0^{2\pi} \mathcal{F}[X](k,\theta;t)d\theta \right\rangle_t,$$

where $\langle\cdot\rangle_t$ stands for the average over time and the usual Fourier transform is expressed in polar coordinates,

$$\mathcal{F}[X](k,\theta;t) = \iint X(\boldsymbol{r};t)e^{-i\boldsymbol{k}\cdot\boldsymbol{r}}d\boldsymbol{r}.$$

Figure 1(a) shows the averaged spatial spectrum in the radial direction, for the experimental data available from the

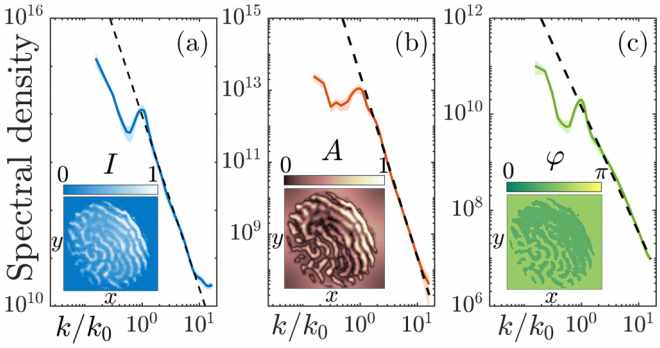

FIG. 1. Spirals turbulentlike regime of a protein concentration on the membrane of a cell (video available from [26]). Averaged spectral density of the concentration field (a), the amplitude (b), and the phase (c). The shaded regions indicate the standard deviations of the temporal distributions. Dashed lines show power-law decays k^p with associated exponents $p = -3.5$ (a), $p = -5.1$ (b), and $p = -2.6$ (c). Insets show instantaneous realizations of the corresponding fields.

Supplemental Material (cf. video S1 in [26]). Note that the recorded intensity is directly related to the concentration of protein. The inset shows a snapshot of the analyzed field. We observe that after a peak corresponding to the (intrinsic) wavelength of the pattern, the concentration spectrum behaves as $\sim k^{-3.5}$. This law is followed over approximately one decade until the intrinsic noise spatial scale is reached, causing the curve to flatten away [27]. This result echoes the work done by Kuramoto and co-workers on turbulencelike behaviors in chemical systems [15]. A physical interpretation was then given in analogy with fluid dynamics: nonlinear coupling is responsible for a connection between different spatial scales and allows for the cascade of a physical quantity through which the chemical system maintains a steady turbulentlike state [14,28]. Here, we see evidence that the smallest (noise-free) scales are connected to scales of the order of the intrinsic wavelength. The experimental limitations prevent from concluding on larger scales behavior. This is because the aspect ratio (as defined by the number of wavelengths the system supports) is generally limited in such experimental data. In the following, we will then limit our analysis to small length scales. By "small," we mean spatial scales smaller than the intrinsic wavelength associated with the traveling wave behavior of the system. Spiral turbulencelike regimes involve many domains of curved wavefronts with more or less random orientations. Such structure is suitable for a decomposition of the field into a constitutive phase and amplitude. This decomposition is performed by means of the conformal monogenic signal [29]. It is constructed based on a generalized Hilbert transform and was developed to analyze local (possibly curved) features of two-dimensional signals. Note that in this decomposition, the phase variable φ varies between 0 and π (see [29] for details). Figures 1(b) and 1(c) show the averaged spectral density in the radial direction associated with the amplitude and phase field (see insets). These spectra similarly exhibit power-law decays with different exponents provided in the caption of Fig. 1. These exponents were obtained by linear regression on the experimental data. We infer that such a power-law behavior of the spectral density is a signature of the turbulentlike dynamics of spirals.

III. MODEL EQUATIONS

To show that the power-law decay in the spectral density observed in the experimental data above is a general feature rather than an exception, we analyze different models. All these models exhibit spirals of different shapes and aspects (see insets of Fig. 2) and span different dynamical regimes, from steadily rotating to meandering and unstable spirals. The only common feature *a priori* is a global spatial disorder and complex dynamics. Numerical simulations are performed on square domains of 512×512 grid points. The laplacians are approximated with second-order accuracy central differences and the time stepping is made by means of a fourth-order Runge-Kutta scheme. Boundary conditions along both spatial directions are considered solid, satisfying the "no-flux" boundary conditions $\partial_{\boldsymbol{n}}\psi = 0$, with $\boldsymbol{n}$ the outward-pointing normal vector at the boundary. First, we study the complex Ginzburg-Landau equation (CGLE) as did the authors of [26] for comparison with their experimental data. The CGLE is a general amplitude equation for any continuous complex field ψ sufficiently close to a Poincaré-Andronov-Hopf bifurcation [30]. As such, it describes coupled nonlinear oscillators, and it is given by

$$\frac{\partial \psi}{\partial t} = \psi - (1+ic)|\psi|^2\psi + D(1+ib)\nabla^2\psi. \qquad (1)$$

This model has been extensively used to describe phase singularities in optics, reaction diffusion, magnetic systems, superconductors, Bose-Einstein condensates, and fluids [30]. Details about spirals dynamics in the CGLE are provided in the Appendix. It is especially shown that for the chosen parameters $b = -0.2$ and $c = 1$, spirals are dynamically stable. It means that no spontaneous front breaking (due for example to Eckhaus or Doppler instability) manifests. The background is also stable.

In the context of reaction diffusion, the Brusselator model is a paradigm for understanding dissipative structures in nonequilibrium systems. It describes the coupled dynamics of the concentrations of two intermediate species involved in a global chemical reaction. The evolution equations read [31]

$$\begin{aligned} \frac{\partial X}{\partial t} &= A - (B+1)X + X^2Y + \nabla^2 X, \\ \frac{\partial Y}{\partial t} &= BX - X^2Y + D\nabla^2 Y. \end{aligned} \qquad (2)$$

A and B are the concentrations of reactants supposed constant and D is the ratio between the diffusion coefficients of species Y and X, respectively. The unique fixed point $(X, Y) = (A, B/A)$ undergoes a Poincaré-Andronov-Hopf bifurcation at $B_c = 1 + A^2$. From this value on, the system locally exhibits a limit cycle whose amplitude gets larger as B grows away from B_c. For our choice of the parameter values $(A = 1, B = 5, D = 0.5)$, the local dynamics is of relaxation oscillations type and spiral waves emerge from the diffusive coupling. For a well-chosen inhomogeneous initial condition, the system exhibits a turbulentlike regime of spirals in which

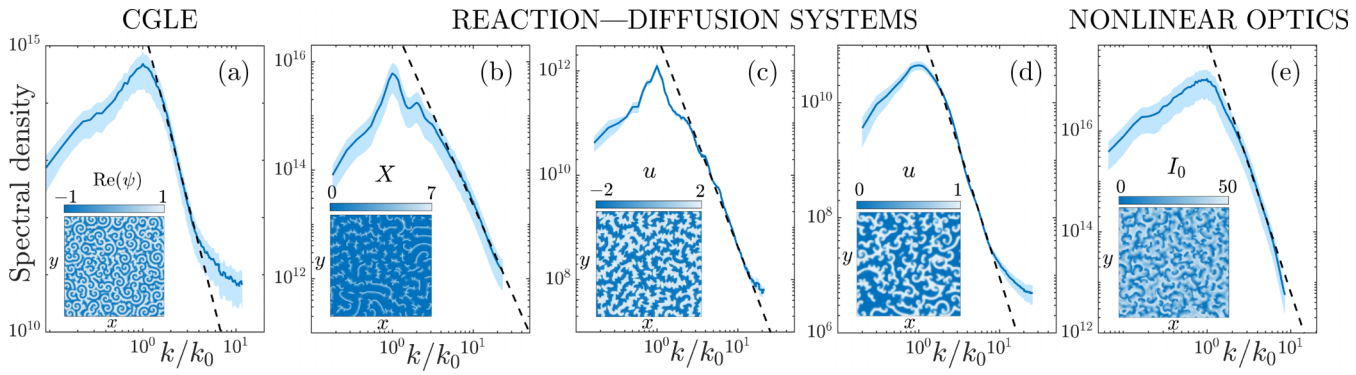

FIG. 2. Spectral density of spiral-forming systems in the turbulentlike regime. Spatial organization for the different models studied, evidencing a general power-law decay k^p of the averaged spectral density at short wavelengths. (a) Coupled oscillators: Complex Ginzburg-Landau equation; (b) reaction diffusion: Brusselator model, excitable systems; (c) FitzHugh-Nagumo equation; and (d) Bär-Eiswirth model; and (e) nonlinear optics. Exponents are found to be $p = -6.36$ (a), $p = -3.37$ (b), $p = -4.05$ (c), $p = -4.48$ (d), and $p = -5.02$ (e). Dashed lines indicate these laws found by linear regression, each with a maximal absolute error of 0.10. The shaded blue regions indicate the standard deviations within the statistical ensemble, and the insets show snapshots of each field in the turbulentlike regime.

the cores diffuse. As for the CGLE, our set of parameters leads to spirals that are dynamically stable. Note however that the diffusion of the cores (called meandering) does not occur in the CGLE.

The FitzHugh-Nagumo model is another paradigm in reaction diffusion systems describing excitable cells, and was originally developed to simulate spike generation in axons [32,33,34]. While the fast variable u stands for the transmembrane potential, v is generally thought of as a slow recovery variable. Here, we consider the slightly different version studied by Winfree [35]:

$$\frac{\partial u}{\partial t} = \frac{1}{\epsilon}\left(u - \frac{u^3}{3} - v\right) + D\nabla^2 u,$$
$$\frac{\partial v}{\partial t} = \epsilon(u + b - gv), \tag{3}$$

with $\epsilon = 0.2$, $b = 0.05$, $g = 0.5$, and $D = 0.2$. Spiral wave solutions then steadily rotate about a fixed center without exhibiting any type of dynamical instability.

Next, considering excitable media, we study the derived Bär-Eiswirth model [36]. It is characterized by delayed inhibitor production and was first used in the context of surface reactions:

$$\frac{\partial u}{\partial t} = -\frac{1}{\epsilon}u(u-1)\left(u - \frac{v+b}{a}\right) + \nabla^2 u,$$
$$\frac{\partial v}{\partial t} = f(u) - v,$$

with

$$f(u) = \begin{cases} 0, & u < 1/3 \\ 1 - 6.75u(u-1)^2, & 1/3 \leqslant u \leqslant 1 \\ 1, & u > 1. \end{cases}$$

The system parameters used in our study are $\epsilon = 0.071$, $a = 0.84$, $b = 0.07$. For these values of the parameters, the individual spiral undergoes the so-called Doppler instability during which spiral breakup occurs in the vicinity of the core, eventually leading to a turbulentlike state where the number of the defects fluctuates.

Finally, nonlinear optical systems were shown to exhibit spiral turbulence [37–41]. One of these, describing an optical parametric oscillator with a saturable absorber, will be used to generalize further the result [42]. Optical parametric oscillators (OPO) are undergoing significant development for the generation of coherent, tunable radiation. We consider a degenerate optical parametric oscillator driven by a coherent field injected at frequency 2ω. A quadratic nonlinear medium converts this field into a field at frequency ω. We add to the optical cavity a saturable absorber that absorbs the field at frequency ω. The effective absorption coefficient depends on the field and is modeled by a two-level saturable medium. We consider the combined effects of diffraction, quadratic nonlinearity, and dissipation. In the mean-field approximation, the optical parametric oscillators with a saturable absorber reads [42,43]

$$\frac{\partial A_0}{\partial t} = -\gamma\left[(1 + i\Delta_0)A_0 + A_1^2 - E\right] + \frac{i}{2}\Delta_\perp A_0,$$
$$\frac{\partial A_1}{\partial t} = -(1 + i\Delta_1)A_1 + A_1^* A_0 - \frac{RA_1}{1 + S|A_1|^2} + i\Delta_\perp A_1.$$

A_0 and A_1 are the normalized slowly varying envelopes of the pump and the signal field at frequencies ω and 2ω, respectively. The injected field amplitude is denoted by E and the ratio of the photon lifetimes at frequencies ω and 2ω is γ. The saturable absorber parameters are the linear loss R and the saturation intensity $1/S$. The transverse Laplacian $\Delta_\perp$ describes the diffraction effect in the transverse plane (x, y). To satisfy the phase matching condition, the ratio between the diffraction coefficients of the two fields is fixed at $1/2$. We consider the pump and the signal field are in perfect resonance with the cavity, $\Delta_0 = \Delta_1 = 0$. We place ourselves in the parameter region where spirals are unstable and spontaneously breakup to form a turbulentlike state. The parameters values are $R = 4.5$, $S = 0.1$, and $E = 7.1$.

IV. RESULTS

On the basis of all the models mentioned above, we carry out a statistical analysis by computing the averaged spatial

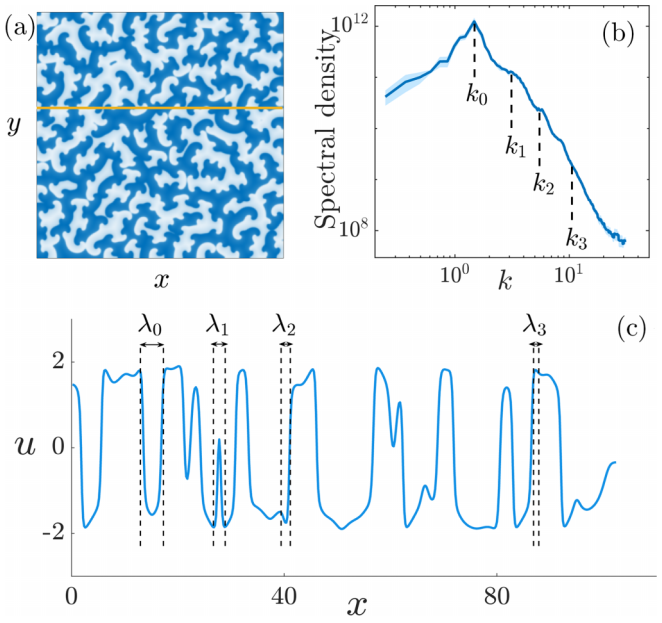

FIG. 3. Small-length structures emerging from the complex interactions of wavefronts. (a) In the FitzHugh-Nagumo model, a random cut (yellow line) is considered from an instantaneous realization of the field $u(x, y, t)$. Typical lengths λ_i are identified in (c) and the corresponding wavenumbers $k_i = 2\pi/\lambda_i$ are located on the averaged spectrum in (b). λ_0 is the intrinsic wavelength emerging from the traveling wave instability.

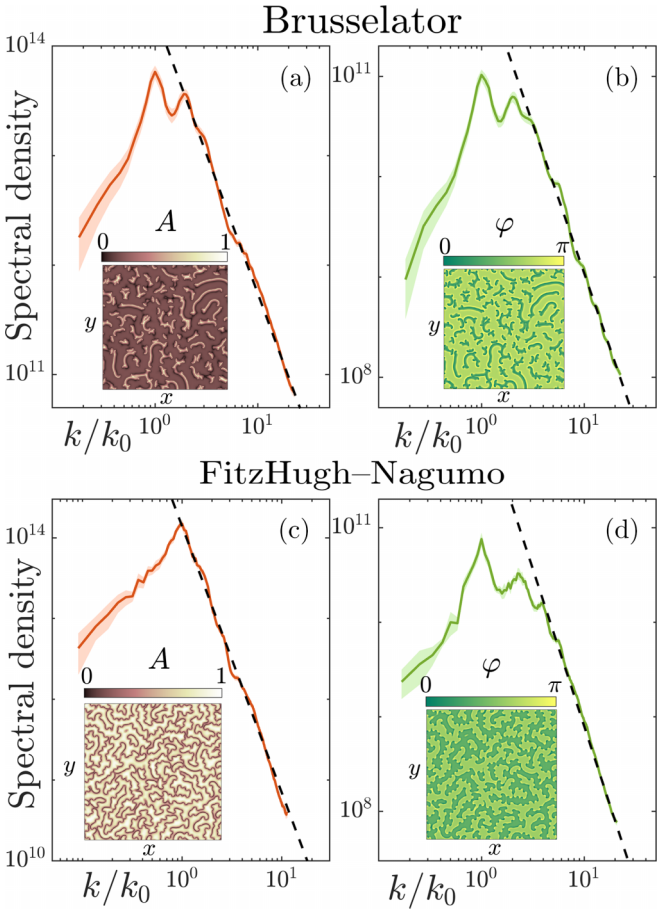

FIG. 4. Power-law decay in the spectral density of the amplitude and phase variables for the Brusselator (top panels) and FitzHugh-Nagumo (bottom panels) model. At small scales, the law k^p is given for the Brusselator model by $p = -2.55 \pm 0.11$ and $p = -2.96 \pm 0.09$ for the amplitude (a) and the phase (b), respectively. For the FitzHugh-Nagumo model, we found $p = -3.30 \pm 0.13$ and $p = -3.32 \pm 0.08$ for the amplitude (c) and the phase (d), respectively. Shaded regions indicate the standard deviation. Insets show corresponding instantaneous fields.

spectral density in the radial direction along with the respective standard deviations. Figure 2 summarizes the results. Despite the differences between the models in the widths, shapes, and general aspects of the spirals (see insets), and in their dynamical regime as discussed in the previous section, the averaged spectrum of each system is characterized by a power-law decay at short wavelengths. For each panel, the local standard deviation of the temporal distribution is indicated as a shaded blue region surrounding the mean value (full line). Note that the averaging procedure has been performed on at least 10 000 frames for every curve. The respective exponents characterizing the decay law are indicated in the caption and are obtained by linear regression over the estimated linear range, with a maximal tolerated error of 0.10. This error is computed as the mean difference between the regression and the "true" value. Discrepancies between the exponents are attributed to the details of the individual spiral shape and dynamics, and quantitative analysis is under investigation.

The occurrence of the power-law at such short wavelengths may find its origin in different mechanisms. However, when the spiral waves are dynamically stable we suggest that it is due to the high density of spirals whose short-range interactions result in irregular spatial modulations of the spiral arms. These modulations introduce new (small) characteristic length scales over which the observable of the system is on average distributed according to the power-law as depicted in Fig. 3. Through this self-organization, a dynamical equilibrium is reached, and the turbulentlike regime is maintained. Figure 3 illustrates the emergence of small-scale structures due to wavefront interactions. In panel (c), several lengths are highlighted on a random cut along the horizontal direction of an instantaneous realization (a) of the u field in the FitzHugh-Nagumo model. This cut is located by a full yellow line. The correspondence with the associated wavenumbers in the spectrum is shown in panel (b) where $k_i = 2\pi/\lambda_i$ ($i = 1, 2, 3$). $k_0 = 2\pi/\lambda_0$ is the asymptotic wavenumber associated with the traveling wave far from the core. It is clear that, in order to construct the spectrum of panel (b), an average over a large statistical ensemble is necessary. Similar results can be obtained from the other models considered in this work. The coupling between the wavenumbers is responsible for the observed power laws on short spatial scales. Although the system also exhibits a global disordered, this analysis focuses on short scales. Our study reveals that at these scales, a common type of spatial self-organization manifests itself in complex regimes of interacting spirals which is independent of the details of the system.

To shed light on the origin of the dynamics observed, we computed the averaged spectra for individual amplitude and

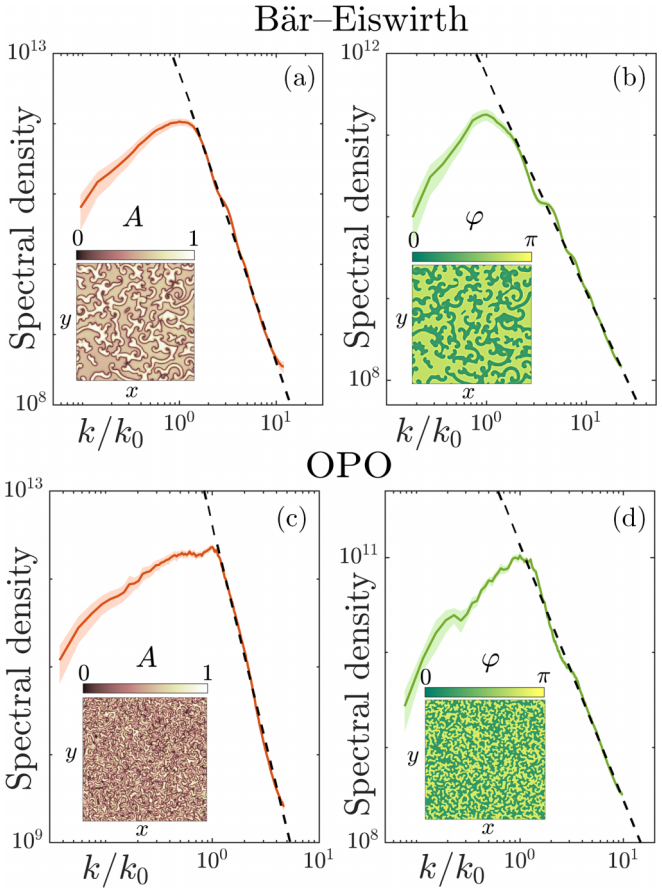

FIG. 5. Power-law decay in the spectral density of the amplitude and phase variables for the Bär-Eiswirth (top panels) and OPO (bottom panels) model. At small scales, the law k^p is given for the Bär-Eiswirth model by $p = -4.09 \pm 0.09$ and $p = -2.64 \pm 0.09$ for the amplitude (a) and the phase (b), respectively. For the OPO model, we found $p = -4.95 \pm 0.09$ and $p = -2.68 \pm 0.08$ for the amplitude (c) and the phase (d), respectively. Shaded regions indicate the standard deviation. Insets show corresponding instantaneous fields.

phase variables from the constructed conformal monogenic signal [20,21]. Results are shown for two reaction-diffusion models in Fig. 4, namely the Brusselator [(a) and (b)] and the FitzHugh-Nagumo model [(c) and (d)]. Each of these spectra exhibits a power-law decay over small scales, as for the associated concentration spectra and similar to what was found from the experimental data. This information takes its importance from the fact that, by construction, these two fields are uncoupled and describe different aspects of the spatiotemporal dynamics. Thus, it is not evident *a priori* that their spectrum will also exhibit power-law decay. The associated exponents are similar to one another but slightly differ from the exponent characterizing the observable. Figure 4 teaches us that both the amplitude and the phase dynamics exhibit similar turbulentlike behavior. Note that a previous work showed power-law behaviors in both these variables but characterized by different exponents associated with different mechanisms [20]. However, this "dynamical decoupling" does not clearly emerge in the turbulentlike regime of spirals for the Brusselator and FitzHugh-Nagumo model. Interestingly, such decoupling is observed in the Bär-Eiswirth and OPO models for which the spiral wave state has undergone a dynamical instability, as shown by Fig. 5. The exponents, indicated in the caption, are significantly different from one another in this case. We also note that the exponents associated with amplitude and phase spectrum for the experimental observations are distinct and that, in this case, the individual spirals are unstable (see [12,26]). A possible interpretation is that spiral instability produces a decoupling between amplitude and phase dynamics. Systematic quantitative investigation is in progress for this hypothesis to be tested. For example, in the case of the CGLE where spirals are stable, we cannot yet explain the difference between the exponents observed.

V. CONCLUSIONS

In conclusion, on the basis of experimental and numerical data, we evidence a general feature of turbulentlike regimes of spirals, namely the power-law decay of the concentration spectral distribution over short spatial scales. This distribution is adopted by the system while maintaining permanent irregular spatiotemporal evolution, and corresponds to a dynamical equilibrium. The numerous interactions of spiral wavefronts result in spatial modulation of the latter and the emergence of structures at scales shorter than the intrinsic wavelength associated with the traveling wave. This explains the domain of extension of the power-law and reveals complexity at short scales. While intrinsic instabilities may play an active role in the dynamics, our work show that they are not a prerequisite for the emergence of power-law spectral distribution. Our result finds its importance in the fact that spiral waves are ubiquitous in nature, in particular in biology and physiology where the turbulentlike dynamics of spirals plays a central role in key processes. On the other hand, the established features of spatiotemporal complex regimes are nowadays still largely restricted to specific settings, and general results bridging different physical systems are necessary. Our work aims to advance in this direction.

ACKNOWLEDGMENT

M.G.C. is thankful for the financial support of ANID-Millenium Science Initiative Program-ICN17_012 (MIRO) and FONDECYT Project No. 1210353. M.T. acknowledges support as Research Director with the Fonds de la Recherche Scientifique FRS-FNRS, Belgium.

APPENDIX: COMPLEX REGIME OF SPIRALS IN THE CGLE

The complex Ginzburg-Landau equation (CGLE) is an amplitude equation that has been derived for many spatially extended close to the Poincaré-Andronov-Hopf bifurcation threshold and is well known to exhibit a wide variety of dynamical behaviors [30]. Among them, a simple spiral solution describes a traveling wave rotating around a phase singularity (spiral core) and takes the form

$$\psi(r,\theta) = F(r)\exp\{i[-\omega t \pm \theta + \phi(r)]\} \qquad \text{(A1)}$$

in the polar coordinates (r,θ). The spiral frequency is ω, and k stands for the asymptotic wavenumber defined in the radial

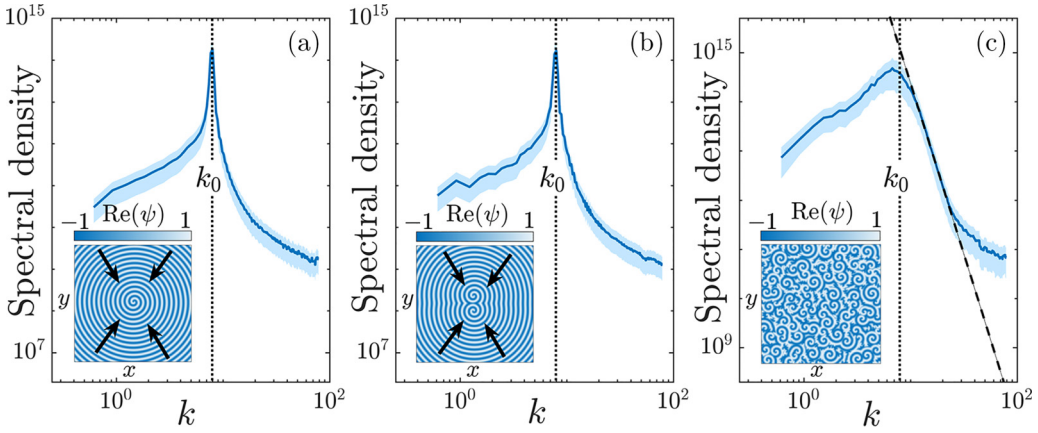

FIG. 6. Averaged spectral density distributions for the Ginzburg-Landau model. Steadily rotating single spiral (a), spiral pair (b), and complex regime (c). For our choices of parameters, the real part of the complex field ψ exhibits wavefronts radially traveling toward the phase singularity as indicated by black arrows in the insets of (a) and (b).

direction. Far from the core, assuming

$$F(r) \underset{r\to\infty}{\longrightarrow} \sqrt{1-k^2} \quad \text{and} \quad \phi(r) \underset{r\to\infty}{\longrightarrow} kr,$$

we find a dispersion relation

$$\omega(k) = (Db - c)k^2 + c.$$

Numerical parameters were taken to be $dx = 0.04$ and $dt = 0.01$ for the spatial and temporal increment, respectively. For the system parameters, we chose the values $b = -0.2$, $c = 1.0$, and $D = 0.003$, for which the group velocity

$$v_g = \frac{\partial\omega}{\partial k} = 2(Db - c)k < 0.$$

The waves then travel toward the singularity as shown in the insets of Figs. 6(a) and 6(b). Note that the asymptotic wavenumber k and the spiral frequency ω are uniquely determined by the parameter values. Figure 6 shows the averaged spectral densities associated with the steadily rotating single spiral (a) and spiral pair (b), and with the complex regime (c) involving many defects. All these results are obtained for the set of parameters specified above. In this regime, spirals are intrinsically stable in the sense that no dynamical instability (such as Eckhaus, Doppler, or phase instability) drives the dynamics, even in the turbulentlike regime. Each spiral steadily rotate around its fixed core and the complex spatial organization is solely due to the high density of defects inducing wavefront interactions. In Fig. 6, the asymptotic wavenumber is numerically identified from the single spiral spectral density (a) to be $k_0 \simeq 7.98$ and is identical for the spiral pair (b). This value is indicated in panel (c) for comparison. We conclude that the associated "natural" wavelength $\lambda_0 = 2\pi/k_0$ still dominates in this complex turbulentlike regime.

Figure 7 depicts the averaged spatial spectra in the radial direction for (i) the amplitude A and (ii) the phase φ variable computed from the conformal monogenic signal (see main text). Insets show examples of instantaneous fields. Similar to what was observed for the Brusselator and FitzHugh-Nagumo model, after a peak at the dominant wavenumber, a power-law decay characterizes the spectral distribution at small wavelengths in both cases. A linear regression in this region gives the exponents -5.03 ± 0.19 for the amplitude and -3.89 ± 0.17 for the phase.

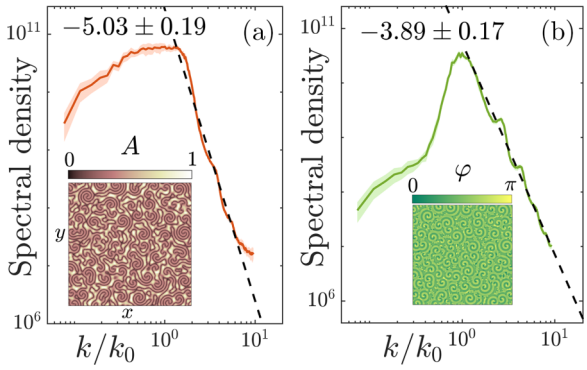

FIG. 7. Averaged spatial spectral density of the amplitude (a) and phase (b) of the CGLE computed from the conformal monogenic signal. A power-law decay characterizes the spectral distribution at small spatial scales as evidenced by the linear regression (dashed line). Insets show instantaneous realizations for each two-dimensional field.

[1] A. T. Winfree, Rotating chemical reactions, Sci. Am. **230**, 82 (1974).

[2] V. S. Zykov, *Simulation of Wave Processes in Excitable Media* (Manchester University Press, Manchester, 1987).

[3] *Spirals and Vortices*, edited by K. Tsuji and C. M. Stefan (Springer, Cham, 2019).

[4] R. A. Gray, A. M. Pertsov, and J. Jalife, Spatial and temporal organization during cardiac fibrillation, Nature (London) **392**, 75 (1998).

[5] S. Alonso, M. Bär, and B. Echebarria, Nonlinear physics of electrical wave propagation in the heart: a review, Rep. Prog. Phys. **79**, 096601 (2016).

[6] X. Huang, W. Xu, J. Liang, K. Takagaki, X. Gao, and J. Y. Wu, Spiral wave dynamics in neocortex, Neuron **68**, 978 (2010).
[7] Y. Xu, X. Long, J. Feng, and P. Gong, Interacting spiral wave patterns underlie complex brain dynamics and are related to cognitive processing, Nat. Hum. Behav. **7**, 1196 (2023).
[8] J. D. Lechleiter and D. E. Clapham, Molecular mechanisms of intracellular calcium excitability in X. laevis oocytes, Cell **69**, 283 (1992).
[9] J. J. Tyson, K. A. Alexander, V. S. Manoranjan, and J. D. Murray, Spiral waves of cyclic AMP in a model of slime mold aggregation, Physica **34**, 193 (1989).
[10] W. M. Bement, M. Leda, A. M. Moe, A. M. Kita, M. E. Larson, A. E. Golding *et al.*, Activator-inhibitor coupling between Rho signalling and actin assembly makes the cell cortex an excitable medium, Nat. Cell Biol. **17**, 1471 (2015).
[11] S. Xiao, C. Tong, Y. Yang, and M. Wu, Mitotic cortical waves predict future division sites by encoding positional and size information, Dev. Cell **43**, 493 (2017).
[12] T. H. Tan, J. Liu, P. W. Miller, M. Tekant, J. Dunkel, and N. Fakhri, Topological turbulence in the membrane of a living cell, Nat. Phys. **16**, 657 (2020).
[13] P. Coullet, L. Gil, and J. Lega, Defect-mediated turbulence, Phys. Rev. Lett. **62**, 1619 (1989).
[14] T. Yamada and Y. Kuramoto, A reduced model showing chemical turbulence, Prog. Theor. Phys. **56**, 681 (1976).
[15] Y. Kuramoto, *Chemical Oscillations, Waves, and Turbulence* (Springer, Berlin, Heidelberg, 1984).
[16] U. Frisch, *Turbulence: The Legacy of AN Kolmogorov* (Cambridge University Press, Cambridge, England, 1995).
[17] E. G. Turitsyna, S. V. Smirnov, S. Sugavanam, N. Tarasov, X. Shu, S. A. Babin, E. V. Podivilov, D. V. Churkin, G. Falkovich, and S. K. Turitsyn, The laminar-turbulent transition in a fibre laser, Nat. Photon. **7**, 783 (2013).
[18] I. R. Roa González, B. C. Lima, P. I. Pincheira, A. A. Brum, A. M. Macêdo, G. L. Vasconcelos, L. de S. Menezes, E. P. Raposo, A. S. Gomes, R. Kashyap, Turbulence hierarchy in a random fibre laser, Nat. Commun. **8**, 15731 (2017).
[19] G. Xu, D. Vocke, D. Faccio, J. Garnier, T. Roger, S. Trillo, and A. Picozzi, From coherent shocklets to giant collective incoherent shock waves in nonlocal turbulent flows, Nat. Commun. **6**, 8131 (2015).
[20] P. J. Aguilera-Rojas, M. G. Clerc, S. Echeverria-Alar, Y. Soupart, and M. Tlidi, Fingerprint pattern bi-turbulence in a driven dissipative optical system, Chaos Solitons Fractals **182**, 114851 (2024).
[21] P. J. Aguilera-Rojas, M. G. Clerc, and S. Navia, Optical feedback-induced spatiotemporal patterns with power law spectra in a liquid crystal light valve, Opt. Lett. **49**, 3292 (2024).
[22] R. Alert, J. Casademunt, and J. F. Joanny, Active turbulence, Annu. Rev. Condens. Matter Phys. **13**, 143 (2022).
[23] K. A. Takeuchi and M. Sano, Universal fluctuations of growing interfaces: Evidence in turbulent liquid crystals, Phys. Rev. Lett. **104**, 230601 (2010).
[24] E. A. L. Henn, J. A. Seman, G. Roati, K. M. Magalhaes, V. S. Bagnato, Emergence of turbulence in an oscillating Bose-Einstein condensate, Phys. Rev. Lett. **103**, 045301 (2009).
[25] S. Ghashghaie, W. Breymann, J. Peinke, P. Talkner, and Y. Dodge, Turbulent cascades in foreign exchange markets, Nature (London) **381**, 767 (1996).
[26] J. Liu, J. F. Totz, P. W. Miller, A. D. Hastewell, Y. C. Chao, J. Dunkel, and N. Fakhri, Topological braiding and virtual particles on the cell membrane, Proc. Natl. Acad. Sci. USA **118**, e2104191118 (2021).
[27] D. E. Sigeti, Survival of deterministic dynamics in the presence of noise and the exponential decay of power spectra at high frequency, Phys. Rev. E **52**, 2443 (1995).
[28] H. Fujisaka and T. Yamada, Theoretical study of a chemical turbulence, Prog. Theor. Phys. **57**, 734 (1977).
[29] L. Wietzke, O. Fleischmann, and G. Sommer, 2D image analysis by generalized Hilbert transforms in conformal space, *European Conference on Computer Vision* (Springer, Berlin Heidelberg, 2008), pp. 638–649.
[30] I. S. Aranson and L. Kramer, The world of the complex Ginzburg-Landau equation, Rev. Mod. Phys. **74**, 99 (2002).
[31] I. Prigogine and R. Lefever, Symmetry breaking instabilities in dissipative systems. II, J. Chem. Phys. **48**, 1695 (1968).
[32] R. FitzHugh, Impulses and physiological states in theoretical models of nerve membrane, Biophys. J. **1**, 445 (1961).
[33] J. Nagumo, S. Arimoto, and S. Yoshizawa, An active pulse transmission line simulating nerve axon, Proc. IRE **50**, 2061 (1962).
[34] C. Rocsoreanu, A. Georgescu, and N. Giurgiteanu, *The FitzHugh-Nagumo Model, Bifuraction and Dynamics* (Springer Science + Business Media, Dordrecht, 2000).
[35] A. T. Winfree, Varieties of spiral wave behavior: An experimentalist's approach to the theory of excitable media, Chaos **1**, 303 (1991).
[36] M. Bär and M. Eiswirth, Turbulence due to spiral breakup in a continuous excitable medium, Phys. Rev. E **48**, R1635 (1993).
[37] P. Coullet, L. Gil, and F. Rocca, Optical vortices, Opt. Commun. **73**, 403 (1989).
[38] D. Yu, W. Lu, and R. G. Harrison, Origin of spiral wave formation in excitable optical systems, Phys. Rev. Lett. **77**, 5051 (1996).
[39] P. Lodahl, M. Bache, and M. Saffman, Spiral intensity patterns in the internally pumped optical parametric oscillator, Phys. Rev. Lett. **85**, 4506 (2000).
[40] S. Longhi, Spiral waves in a class of optical parametric oscillators, Phys. Rev. E **63**, 055202(R) (2001).
[41] M. Le Berre, E. Ressayre, A. Tallet, and M. Tlidi, Spiral patterns, spiral breakup, and zigzag spirals in an optical device, Phys. Rev. E **71**, 036224 (2005).
[42] M. Tlidi and P. Mandel, Space-time localized structures in the degenerate optical parametric oscillator, Phys. Rev. A **59**, 2575(R) (1999).
[43] M. Tlidi, M. Haelterman, and P. Mandel, Spatiotemporal patterns and localized structures in nonlinear optics, Phys. Rev. E **56**, 6524 (1997).